Chemical Engineering Science 78 (2012) 155–166

Contents lists available at SciVerse ScienceDirect

Chemical Engineering Science

journal homepage: www.elsevier.com/locate/ces

Fault detection and isolation and fault tolerant control of a catalytic alkylation of benzene process

David Chilin [a], Jinfeng Liu [b], Xianzhong Chen [a], Panagiotis D. Christofides [a,c,*]

[a] Department of Chemical and Biomolecular Engineering, University of California, Los Angeles, CA 90095-1592, USA
[b] Department of Chemical & Materials Engineering, University of Alberta, Edmonton, Canada AB T6G 2V4
[c] Department of Electrical Engineering, University of California, Los Angeles, CA 90095-1592, USA

HIGHLIGHTS

- Fault detection and isolation method for alkylation of benzene process.
- Fault tolerant control strategies for alkylation of benzene process.
- Detailed simulation study of various monitoring and control strategies.

ARTICLE INFO

Article history:
Received 5 April 2012
Received in revised form
12 May 2012
Accepted 14 May 2012
Available online 24 May 2012

Keywords:
Process control
Fault-tolerant control
Model predictive control
Process simulation
Process control
Process design

ABSTRACT

In this work, we focus on the application of an integrated fault detection and isolation and fault tolerant control (FDIFTC) framework to a catalytic alkylation of benzene process. We consider that the catalytic alkylation of benzene process is controlled by a distributed model predictive control (DMPC) system and is subjected to unknown, persistent actuator faults. The FDIFTC system monitors closed-loop process residuals in order to detect and isolate a faulty actuator. After isolation of an actuator fault, the FDIFTC system estimates the fault magnitude, recalculates a new optimal operating point, and ultimately reconfigures the DMPC system to maintain stability of the process in an optimal manner. Extensive simulations are carried out to demonstrate the performance of the FDIFTC system from closed-loop stability and performance points of view.

1. Introduction

World markets are becoming increasingly competitive, such that manufacturers are driven to pursue every bit of performance gain from current operations in order to maintain competitiveness. In the pursuit of this ultimate performance, manufacturers are increasingly relying on advanced process control systems. With advances constantly being made in computational capabilities, model predictive control (MPC) has emerged as a reasonable and potentially profitable solution to achieve optimal process operation and control. MPC lends itself well as an overlying layer that can be implemented on top of existing classical plant control systems and does well to handle input and state constraints. As the complexity of manufacturing plants has increased, cooperative, distributed MPC architectures have emerged that also deal well with plant modernization that may include sensor and actuator networks that may be implemented using wireless or wired networks.

One of the largest pitfalls for performance are abnormal situations which account for at least $20 billion in lost revenue annually in the United States alone. In this context, an added advantage of MPC is the ability to handle constraints such that when combined with fault tolerant control strategies introduces flexibility and optimization that can not only avert disaster in the case of an abnormal situation but also maintain optimal plant operation. Recently, distributed MPC (DMPC) has attracted a lot of attention because of its advantages in control model maintenance, computational complexity and fault tolerance. In the context of DMPC designs, several DMPC schemes have been proposed in the literature that deal with the coordination of separate MPC controllers that communicate in order to obtain optimal input trajectories in a distributed manner; see Camponogara et al. (2002), Rawlings and Stewart (2008), Scattolini (2009), Liu et al. (2010), Liu et al. (2009), Christofides et al. (2012) for results in this area.

* Corresponding author at: Department of Chemical and Biomolecular Engineering, University of California, Los Angeles, CA 90095-1592, USA. Tel.: +1 310 794 1015; fax: +1 310 206 4107.
E-mail address: pdc@seas.ucla.edu (P.D. Christofides).

0009-2509/$ - see front matter © 2012 Elsevier Ltd. All rights reserved.
http://dx.doi.org/10.1016/j.ces.2012.05.015

Considering the increasing complexity of modern chemical processes and the corresponding increase in controller complexity, there is a broad array of abnormal events that may occur in a chemical process and/or its control system. Fault detection and isoaltion and fault tolerant control (FDIFTC) goes hand in hand with the increasing complexities as more sophisticated methods are needed to manage abnormal situations. In the context of problems that FDIFTC may address, initial efforts focused on cases where actuator faults considered had redundant components with the option of shutting down the faulty components upon isolation and activating functioning components guaranteeing closed-loop stability, as in Mhaskar et al. (2006). Subsequently, different isolation methods were developed to improve effectiveness and speed of fault isolation which in turn broadened the range of recoverable faults as in Chilin et al. (2010) where the fault-tolerant control (FTC) system relied only on the remaining control actuators to achieve FTC. In Chilin et al. (2012), another step was made in the direction of FDIFTC, where the concept of fault isolation windows was utilized to further expand the range of recoverable actuator faults considered in previous works. Other recent work has focused on the development of an agent-based approach to process monitoring and fault-tolerant control (Tatara et al., 2007; Perk et al., 2010).

The focus of this paper is on the application of an integrated FDIFTC framework to a catalytic alkylation of benzene process which is controlled by a DMPC system and is subjected to unknown, persistent control actuator faults. The FDIFTC system uses measurements of process variables like temperature and concentrations. To design the fault detection and isolation (FDI) system we take advantage of recent results on FDI (Chilin et al., 2012). After isolation of an actuator fault, the FDIFTC system estimates the fault magnitude, recalculates a new optimal operating point, and ultimately reconfigures the DMPC system to maintain stability of the process in an optimal manner. Extensive simulations are carried out to demonstrate the effectiveness of the FDIFTC system from stability and performance points of view.

2. Description of the Alkylation of Benzene process

The process of alkylation of benzene with ethylene to produce ethylbenzene is widely used in the petrochemical industry. Dehydration of the product produces styrene, which is the precursor to polystyrene and many copolymers. The process model developed in this section is based on these references Ganji et al. (2004), Lee (2005), Perego and Ingallina (2004), Woodle (2006), You et al. (2006) and details can be found in Liu et al. (2010). In the remainder, we review this model for completeness of the presentation and of the results of this work. More specifically, the process considered in this work consists of four continuously stirred tank reactors (CSTRs) and a flash tank separator, as shown in Fig. 1. The CSTR-1, CSTR-2 and CSTR-3 are in series and involve the alkylation of benzene with ethylene. Pure benzene is fed from stream F_1 and pure ethylene is fed from streams F_2, F_4 and F_6. Two catalytic reactions take place in CSTR-1, CSTR-2 and CSTR-3. Benzene (A) reacts with ethylene (B) and produces the required product ethylbenzene (C) (reaction 1); ethylbenzene can further react with ethylene to form 1,3-diethylbenzene (D) (reaction 2) which is the byproduct. The effluent of CSTR-3, including the products and leftover reactants, is fed to a flash tank separator, in which most of benzene is separated overhead by vaporization and condensation techniques and recycled back to the plant and the bottom product stream is removed. A portion of the recycle stream F_{r2} is fed back to

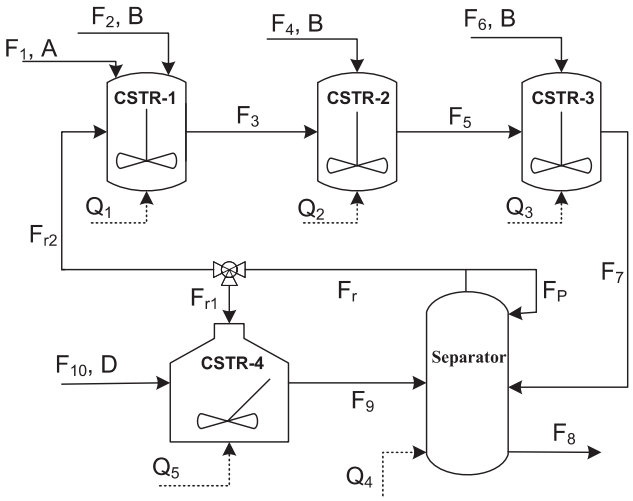

Fig. 1. Process flow diagram of alkylation of benzene.

CSTR-1 and another portion of the recycle stream F_{r1} is fed to CSTR-4 together with an additional feed stream F_{10} which contains 1,3-diethylbenzene from further distillation process that we do not consider in this example. In CSTR-4, reaction 2 and catalyzed transalkylation reaction in which 1,3-diethylbenzene reacts with benzene to produce ethylbenzene (reaction 3) takes place. All chemicals left from CSTR-4 eventually pass into the separator. All the materials in the reactions are in liquid phase due to high pressure. The dynamic equations describing the behavior of the process, obtained through material and energy balances under standard modeling assumptions, are shown below:

$$\frac{dC_{A1}}{dt} = \frac{F_1C_{A0}+F_{r2}C_{Ar}-F_3C_{A1}}{V_1} - r_1(T_1,C_{A1},C_{B1}) \tag{1a}$$

$$\frac{dC_{B1}}{dt} = \frac{F_2C_{B0}+F_{r2}C_{Br}-F_3C_{B1}}{V_1} - r_1(T_1,C_{A1},C_{B1}) - r_2(T_1,C_{B1},C_{C1}) \tag{1b}$$

$$\frac{dC_{C1}}{dt} = \frac{F_{r2}C_{Cr}-F_3C_{C1}}{V_1} + r_1(T_1,C_{A1},C_{B1}) - r_2(T_1,C_{B1},C_{C1}) \tag{1c}$$

$$\frac{dC_{D1}}{dt} = \frac{F_{r2}C_{Dr}-F_3C_{D1}}{V_1} + r_2(T_1,C_{B1},C_{C1}) \tag{1d}$$

$$\frac{dT_1}{dt} = \frac{Q_1+F_1C_{A0}H_A(T_{A0})+F_2C_{B0}H_B(T_{B0})}{\sum_i^{A,B,C,D} C_{i1}C_{pi}V_1} + \frac{\sum_i^{A,B,C,D}(F_{r2}C_{ir}H_i(T_4)-F_3C_{i1}H_i(T_1))}{\sum_i^{A,B,C,D} C_{i1}C_{pi}V_1} + \frac{(-\Delta H_{r1})r_1(T_1,C_{A1},C_{B1})(-\Delta H_{r2})r_2(T_1,C_{B1},C_{C1})}{\sum_i^{A,B,C,D} C_{i1}C_{pi}} \tag{1e}$$

$$\frac{dC_{A2}}{dt} = \frac{F_3C_{A1}-F_5C_{A2}}{V_2} - r_1(T_2,C_{A2},C_{B2}) \tag{1f}$$

$$\frac{dC_{B2}}{dt} = \frac{F_3C_{B1}+F_4C_{B0}-F_5C_{B2}}{V_2} - r_1(T_2,C_{A2},C_{B2}) - r_2(T_2,C_{B2},C_{C2}) \tag{1g}$$

$$\frac{dC_{C2}}{dt} = \frac{F_3C_{C1}-F_5C_{C2}}{V_2} + r_1(T_2,C_{A2},C_{B2}) - r_2(T_2,C_{B2},C_{C2}) \tag{1h}$$

$$\frac{dC_{D2}}{dt} = \frac{F_3C_{D1}-F_5C_{R2}}{V_2} + r_2(T_2,C_{B2},C_{C2}) \tag{1i}$$

$$\frac{dT_2}{dt} = \frac{Q_2 + F_4 C_{B0} H_B(T_{B0})}{\sum_i^{A,B,C,D} C_{i2} C_{pi} V_2} + \frac{\sum_i^{A,B,C,D} (F_3 C_{i1} H_i(T_1) - F_5 C_{i2} H_i(T_2))}{\sum_i^{A,B,C,D} C_{i2} C_{pi} V_2} + \frac{(-\Delta H_{r1}) r_1(T_2, C_{A2}, C_{B2}) (-\Delta H_{r2} r_2)(T_2, C_{A2}, C_{B2})}{\sum_i^{A,B,C,D} C_{i2} C_{pi}} \quad (1j)$$

$$\frac{dC_{A3}}{dt} = \frac{F_5 C_{A2} - F_7 C_{A3}}{V_3} - r_1(T_3, C_{A3}, C_{B3}) \quad (1k)$$

$$\frac{dC_{B3}}{dt} = \frac{F_5 C_{B2} + F_6 C_{B0} - F_7 C_{B3}}{V_3} - r_1(T_3, C_{A3}, C_{B3}) - r_2(T_3, C_{B3}, C_{C3}) \quad (1l)$$

$$\frac{dC_{C3}}{dt} = \frac{F_5 C_{C2} - F_7 C_{C3}}{V_3} + r_1(T_3, C_{A3}, C_{B3}) - r_2(T_3, C_{B3}, C_{C3}) \quad (1m)$$

$$\frac{dC_{D3}}{dt} = \frac{F_5 C_{D2} - F_7 C_{D3}}{V_3} + r_2(T_3, C_{B3}, C_{C3}) \quad (1n)$$

$$\frac{dT_3}{dt} = \frac{Q_3 + F_6 C_{B0} H_B(T_{B0})}{\sum_i^{A,B,C,D} C_{i3} C_{pi} V_3} + \frac{\sum_i^{A,B,C,D} (F_5 C_{i2} H_i(T_2) - F_7 C_{i3} H_i(T_3))}{\sum_i^{A,B,C,D} C_{i3} C_{pi} V_3} + \frac{(-\Delta H_{r1}) r_1(T_3, C_{A3}, C_{B3}) (-\Delta H_{r2}) r_2(T_3, C_{B3}, C_{C3})}{\sum_i^{A,B,C,D} C_{i3} C_{pi}} \quad (1o)$$

$$\frac{dC_{A4}}{dt} = \frac{F_7 C_{A3} + F_9 C_{A5} - F_r C_{Ar} - F_8 C_{A4}}{V_4} \quad (1p)$$

$$\frac{dC_{B4}}{dt} = \frac{F_7 C_{B3} + F_9 C_{B5} - F_r C_{Br} - F_8 C_{B4}}{V_4} \quad (1q)$$

$$\frac{dC_{C4}}{dt} = \frac{F_7 C_{C3} + F_9 C_{C5} - F_r C_{Cr} - F_8 C_{C4}}{V_4} \quad (1r)$$

$$\frac{dC_{D4}}{dt} = \frac{F_7 C_{D3} + F_9 C_{D5} - F_r C_{Dr} - F_8 C_{D4}}{V_4} \quad (1s)$$

$$\frac{dT_4}{dt} = \frac{Q_4 + \sum_i^{A,B,C,D} (F_7 C_{i3} H_i(T_3) + F_9 C_{i5} H_i(T_5))}{\sum_i^{A,B,C,D} C_{i4} C_{pi} V_4} + \frac{\sum_i^{A,B,C,D} (-M_i H_i(T_4) - F_8 C_{i4} H_i(T_4) - M_i H_{vapi})}{\sum_i^{A,B,C,D} C_{i4} C_{pi} V_4} \quad (1t)$$

$$\frac{dC_{A5}}{dt} = \frac{F_{r1} C_{Ar} - F_9 C_{A5}}{V_5} - r_3(T_5, C_{A5}, C_{D5}) \quad (1u)$$

$$\frac{dC_{B5}}{dt} = \frac{F_{r1} C_{Br} - F_9 C_{B5}}{V_5} - r_2(T_5, C_{B5}, C_{C5}) \quad (1v)$$

$$\frac{dC_{C5}}{dt} = \frac{F_{r1} C_{Cr} - F_9 C_{C5}}{V_5} - r_2(T_5, C_{B5}, C_{C5}) + 2r_3(T_5, C_{A5}, C_{D5}) \quad (1w)$$

$$\frac{dC_{D5}}{dt} = \frac{F_{r1} C_{Dr} + F_{10} C_{D0} - F_9 C_{D5}}{V_5} + r_2(T_5, C_{B5}, C_{C5}) - r_3(T_5, C_{A5}, C_{D5}) \quad (1x)$$

$$\frac{dT_5}{dt} = \frac{Q_5 + F_{10} C_{D0} H_D(T_{D0})}{\sum_i^{A,B,C,D} C_{i5} C_{pi} V_5} + \frac{\sum_i^{A,B,C,D} (F_{r1} C_{ir} H_i(T_4) - F_9 C_{i5} H_i(T_5))}{\sum_i^{A,B,C,D} C_{i5} C_{pi} V_5} + \frac{(-\Delta H_{r2}) r_2(T_5, C_{B5}, C_{C5}) (-\Delta H_{r3}) r_3(T_5, C_{A5}, C_{D5})}{\sum_i^{A,B,C,D} C_{i5} C_{pi}} \quad (1y)$$

where r_1, r_2 and r_3 are the reaction rates of reactions 1, 2 and 3 respectively and H_i, $i=A, B, C, D$, are the enthalpies of the reactants. The reaction rates are related to the concentrations of the reactants and the temperature in each reactor as follows:

$$r_1(T, C_A, C_B) = 0.0840 e^{-9502/RT} C_A^{0.32} C_B^{1.5} \quad (2)$$

$$r_2(T, C_B, C_C) = \frac{0.0850 e^{-20643/RT} C_B^{2.5} C_C^{0.5}}{(1 + k_{EB2} C_D)} \quad (3)$$

$$r_3(T, C_A, C_D) = \frac{66.1 e^{-61280/RT} C_A^{1.0218} C_D}{(1 + k_{EB3} C_A)} \quad (4)$$

where:

$$k_{EB2} = 0.152 e^{-3933/RT} \quad (5)$$

$$k_{EB3} = 0.490 e^{-50870/RT}. \quad (6)$$

The heat capacities of the species are assumed to be constants and the molar enthalpies have a linear dependence on temperature as follows:

$$H_i(T) = H_{iref} + C_{pi}(T - T_{ref}), \quad i = A,B,C,D \quad (7)$$

where C_{pi}, $i=A, B, C, D$ are heat capacities.

The model of the flash tank separator is developed under the assumption that the relative volatility of each species has a linear correlation with the temperature of the vessel within the operating temperature range of the flash tank, as shown below:

$$\alpha_A = 0.0449 T_4 + 10 \quad (8)$$

$$\alpha_B = 0.0260 T_4 + 10 \quad (9)$$

$$\alpha_C = 0.0065 T_4 + 0.5 \quad (10)$$

$$\alpha_D = 0.0058 T_4 + 0.25 \quad (11)$$

where α_i, $i=A, B, C, D$, represent the relative volatilities. It has also been assumed that there is a negligible amount of reaction taking place in the separator and a fraction of the total condensed overhead flow is recycled back to the reactors. The following algebraic equations model the composition of the overhead stream relative to the composition of the liquid holdup in the flash tank:

$$M_i = k \frac{\alpha_i (F_7 C_{i3} + F_9 C_{i5}) \sum_j^{A,B,C,D} (F_7 C_{j3} + F_9 C_{j5})}{\sum_j^{A,B,C,D} \alpha_j (F_7 C_{j3} + F_9 C_{j5})} \quad i = A,B,C,D \quad (12)$$

where M_i, $i=A, B, C, D$ are the molar flow rates of the overhead reactants and k is the fraction of condensed overhead flow recycled to the reactors. Based on M_i, $i=A, B, C, D$, we can calculate the concentration of the reactants in the recycle streams as follows:

$$C_{ir} = \frac{M_i}{\sum_j^{A,B,C,D} M_i / C_{j0}}, \quad i = A,B,C,D \quad (13)$$

where C_{j0}, $j=A, B, C, D$, are the mole densities of pure reactants. The condensation of vapor takes place overhead, and a portion of the condensed liquid is purged back to separator to keep the flow rate of the recycle stream at a fixed value. The temperature of the condensed liquid is assumed to be the same as the temperature of the vessel.

The definitions for the variables used in the above model can be found in Table 1, with the parameter values given in Table 2.

Each of the tanks has an external heat/coolant input. The manipulated inputs to the process are the heat injected to or removed from the five vessels, Q_1, Q_2, Q_3, Q_4 and Q_5, and the feed stream flow rates to CSTR-2 and CSTR-3, F_4 and F_6.

The states of the process consist of the concentrations of A, B, C, D in each of the five vessels and the temperatures of the vessels. The state of the process is assumed to be available continuously to the controllers. We consider a stable steady state (operating point), x_s, of the process which is defined by the steady-state inputs Q_{1s}, Q_{2s}, Q_{3s}, Q_{4s}, Q_{5s}, F_{4s} and F_{6s} which are shown in Table 3. The steady-state temperatures in the five vessels are the

Table 1
Process variables.

C_{A1}, C_{B1}, C_{C1}, C_{D1}	Concentrations of *A,B,C,D* in CSTR-1
C_{A2}, C_{B2}, C_{C2},C_{D2}	Concentrations of *A,B,C,D* in CSTR-2
C_{A3}, C_{B3}, C_{C3}, C_{D3}	Concentrations of *A,B,C,D* in CSTR-3
C_{A4}, C_{B4}, C_{C4}, C_{D4}	Concentrations of *A,B,C,D* in separator
C_{A5}, C_{B5}, C_{C5}, C_{D5}	Concentrations of *A,B,C,D* in CSTR-4
C_{Ar}, C_{Br}, C_{Cr}, C_{Dr}	Concentrations of *A,B,C,D* in F_r
T_1, T_2, T_3, T_4, T_5	Temperatures in each vessel
T_{ref}	Reference temperature
F_3, F_5, F_7, F_8, F_9	Effluent flow rates from each vessel
F_1, F_2, F_4, F_6, F_{10}	Feed flow rates to each vessel
F_r, F_{r1}, F_{r2}	Recycle flow rates
H_{vapA}, H_{vapB}	Enthalpies of vaporization of *A,B*
H_{vapC}, H_{vapD}	Enthalpies of vaporization of *C,D*
H_{Aref}, H_{Bref}	Enthalpies of *A*, *B* at T_{ref}
H_{Cref}, H_{Dref}	Enthalpies of *C*, *D* at T_{ref}
ΔH_{r1}, ΔH_{r2}, ΔH_{r3}	Heat of reactions 1, 2 and 3
V_1, V_2, V_3, V_4, V_5	Volume of each vessel
Q_1, Q_2, Q_3, Q_4, Q_5	External heat/coolant inputs to each vessel
C_{pA}, C_{pB}, C_{pC}, C_{pD}	Heat capacity of *A*, *B*, *C*, *D*
α_A, α_B, α_C, α_D	Relative volatilities of *A*, *B*, *C*, *D*
C_{A0}, C_{B0}, C_{C0}, C_{D0}	Molar densities of pure *A*, *B*, *C*, *D*
T_{A0}, T_{B0}, T_{D0}	Feed temperatures of pure *A*, *B*, *D*
k	Fraction of overhead flow recycled to the reactors

Table 2
Parameter values.

$F_1 = 7.1 \times 10^{-3}$ m^3/s	$F_r = 0.012$ m^3/s
$F_2 = 8.697 \times 10^{-4}$ m^3/s	$F_{r1} = 0.006$ m^3/s
$F_{r2} = 0.006$ m^3/s	$V_1 = 1$ m^3
$F_1 0 = 2.31 \times 10^{-3}$ m^3/s	$V_2 = 1$ m^3
$H_{vapA} = 3.073 \times 10^4$ J/mol	$V_3 = 1$ m^3
$H_{vapB} = 1.35 \times 10^4$ J/mol	$V_4 = 3$ m^3
$H_{vapC} = 4.226 \times 10^4$ J/mol	$V_5 = 1$ m^3
$H_{vapD} = 4.55 \times 10^4$ J/mol	$C_{pA} = 184.6$ J/mol K
$\Delta H_{r1} = -1.536 \times 10^5$ J/mol	$C_{pB} = 59.1$ J/mol K
$\Delta H_{r2} = -1.118 \times 10^5$ J/mol	$C_{pC} = 247$ J/mol K
$\Delta H_{r3} = 4.141 \times 10^5$ J/mol	$C_{pD} = 301.3$ J/mol K
$C_{A0} = 1.126 \times 10^4$ mol/m^3	$T_{ref} = 450$ K
$C_{B0} = 2.028 \times 10^4$ mol/m^3	$T_{A0} = 473$ K
$C_{C0} = 8174$ mol/m^3	$T_{B0} = 473$ K
$C_{D0} = 6485$ mol/m^3	$T_{D0} = 473$ K
$k = 0.8$	

Table 3
Steady-state input values for x_s.

Q_{1s}	-4.4×10^6 J/s	Q_{2s}	-4.6×10^6 J/s
Q_{3s}	-4.7×10^6 J/s	Q_{4s}	9.2×10^6 J/s
Q_{5s}	5.9×10^6 J/s	F_{4s},F_{6s}	8.697×10^{-4} m^3/s

Table 4
Manipulated input constraints.

$\lvert u_{11}\rvert \le 7.5 \times 10^5$ J/s	$\lvert u_{1i}\rvert \le 5 \times 10^5$ J/s,$(i = 2, 3)$
$\lvert u_{21}\rvert \le 6 \times 10^5$ J/s	$\lvert u_{22}\rvert \le 5 \times 10^5$ J/s
$\lvert u_{31}\rvert \le 4.93 \times 10^{-5}$ m^3/s	$\lvert u_{32}\rvert \le 4.93 \times 10^{-5}$ m^3/s

following:

$T_{1s} = 477.2K$, $T_{2s} = 476.9K$, $T_{3s} = 473.4K$,$T_{4s} = 470.6K$, $T_{5s} = 478.2K$.

The process will be under the control of three distributed Lyapunov-based model predictive controllers. The first distributed controller (LMPC 1) will control the values of Q_1, Q_2 and Q_3, the second distributed controller (LMPC 2) will decide the values of Q_4 and Q_5, and the third distributed controller (LMPC 3) will decide the values of F_4 and F_6. The manipulated inputs for LMPC 1, 2, and 3 will use deviation variables and be described by the sets $u_1^T = [u_{11}\ u_{12}\ u_{13}] = [Q_1 - Q_{1s}\ Q_2 - Q_{2s}\ Q_3 - Q_{3s}]$, $u_2^T = [u_{21}\ u_{22}] = [Q_4 - Q_{4s}\ Q_5 - Q_{5s}]$ and $u_3^T = [u_{31}\ u_{32}] = [F_4 - F_{4s}\ F_6 - F_{6s}]$ which are subjected to the constraints shown in Table 4.

The alkylation of benzene process model of Eq. (1) belongs to the following class of nonlinear systems

$$\dot{x}(t) = f(x(t)) + \sum_{i=1}^{3} g_i(x(t))u_i(t) \tag{14}$$

where $x(t) \in R^{25}$ denotes the vector of process state variables. The explicit expressions of f, g_i $(i = 1,2,3)$ are omitted for brevity. We assume that the state x of the system is sampled synchronously and the time instants at which state measurements are sampled is indicated by the time sequence $\{t_{k \ge 0}\}$ with $t_k = t_0 + k\Delta$, $k = 0, 1, \ldots$ where t_0 is the initial time and $\Delta = 15$ s is the sampling time.

In the control of the process, u_1 and u_2 are necessary to keep the stability of the closed-loop system, while u_3 can be used as an extra manipulated input to improve the closed-loop performance. We can design a Lyapunov-based controller $h(x) = [h_1(x)\ h_2(x)\ h_3(x)]^T$ to stabilize the closed-loop process. Specifically, $h_1(x)$ and $h_2(x)$ are designed as follows (Sontag, 1989):

$$h_i(x) = \begin{cases} -\dfrac{L_f V + \sqrt{(L_f V)^2 + (L_{g_i} V)^4}}{(L_{g_i} V)^2} L_{g_i} V & \text{if } L_{g_i} V \neq 0 \\ 0 & \text{if } L_{g_i} V = 0 \end{cases}$$

where $i = 1, 2$, $L_f V = \partial V / \partial x f(x)$ and $L_{g_i} V = \partial V / \partial x g_i(x)$ denote the Lie derivatives of the scalar function V with respect to the vector fields f and g_i $(i = 1, 2)$, respectively. The controller $h_3(x)$ is chosen to be $h_3(x) = [0\ 0]^T$ because the input set u_3 is not needed to stabilize the process. We consider a Lyapunov function $V(x) = x^T P x$ with P being the following weight matrix: $P = \mathrm{diag}([1\ 1\ 1\ 1\ 10\ 1\ 1\ 1\ 1\ 10\ 1\ 1\ 1\ 1\ 10\ 1\ 1\ \ 1\ 1\ 10\ 1\ 1\ 1\ 1\ 10])$.[1] The values of the weights in P have been chosen in such a way that the Lyapunov-based controller $h(x)$ stabilizes the closed-loop system asymptotically and provides good closed-loop performance.

3. FDIFTC system design

3.1. Fault-free DMPC system design

In this section, we design the fault-free control system for the alkylation process following the sequential distributed Lyapunov-based MPC (LMPC) approach described in Liu et al. (2009,2010). Specifically, for the alkylation process, we design three LMPC controllers to compute u_1, u_2, and u_3, respectively. In the sequential distributed control scheme, the distributed LMPCs communicate in a one-directional manner as shown in Fig. 2 in which at each sampling time t_k: (1) all LMPCs receive the state measurement $x(t_k)$ from the sensors; (2) LMPC 3 evaluates the optimal input trajectory of u_3 and sends its future input information to LMPC 2; (3) LMPC 2 evaluates its optimal input trajectory of u_2 and sends its own and LMPC 3's future input information to LMPC 1; (4) LMPC 1 evaluates its optimal input trajectory of u_1; and (5) the first step input values of u are sent to its corresponding actuators and the process is repeated at every sampling time.

[1] *diag*(v) denotes a matrix with its diagonal elements being the elements of vector v and all the other elements being zeros.

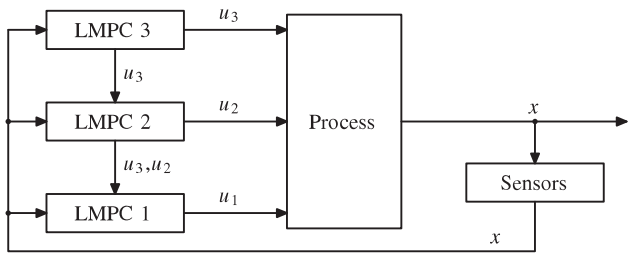

Fig. 2. Sequential distributed LMPC for the catalytic alkylation of benzene process.

The sequential DMPC is based on $h(x)$ and the Lyapunov function $V(x)$. Specifically, the distributed LMPCs are based on the following optimization problem:

$$\min_{u_i \in S(\Delta)} \int_0^{N\Delta} [\tilde{x}(\tau)^T Q_c \tilde{x}(\tau) + \sum_{i=1}^{3} u_i(\tau)^T R_{ci} u_i(\tau)]\, d\tau \tag{15a}$$

$$\text{s.t.} \quad \dot{\tilde{x}}(\tau) = f(\tilde{x}(\tau)) + \sum_{i=1}^{3} g_i(\tilde{x}(\tau)) u_i(\tau) \tag{15b}$$

$$u_j(\tau) = h_k(\tilde{x}(b\Delta)), \quad \forall \tau \in [b\Delta,(b+1)\Delta),\ b = 0,\ldots,N-1,\ j = 1,\ldots,i-1 \tag{15c}$$

$$u_j(\tau) = u_j^*(\tau | t_k), \quad j = i+1,\ldots,3 \tag{15d}$$

$$\tilde{x}(0) = x(t_k) \tag{15e}$$

$$u_i(\tau) \in U_i \tag{15f}$$

$$\frac{\partial V(x)}{\partial x} g_i(x(t_k)) u_i(0) \le \frac{\partial V(x)}{\partial x} g_i(x(t_k)) h_i(x(t_k)) \tag{15g}$$

where $S(\Delta)$ is the family of piece-wise continuous functions with sampling time Δ, the prediction horizon $N=3$, $\tilde{x}$ is the predicted system trajectory, u_j^* is the future optimal input trajectory calculated by LMPC j, Q_c and R_{ci} are positive definite weighting matrices with the following values: $Q_c = \text{diag}(Q_v)$ with $Q_v = [1\ 1\ 1\ 1\ 10^3\ 1\ 1\ 1\ 1\ 10^3\ 10\ 10\ 10\ 10\ 10^4\ 1\ 1\ 1\ 1\ 10^3\ 1\ 1\ 1\ 1\ 10^3]$ and $R_{c1} = \text{diag}([10^{-8}\ 10^{-8}\ 10^{-8}])$, $R_{c2} = \text{diag}([10^{-8}\ 10^{-8}])$ and $R_{c3} = \text{diag}([1\ 1])$.

The optimal solution to this optimization problem is denoted by $u_i^*(\tau | t_k)$, $i=1,2,3$, which is defined for $\tau \in [0,N\Delta]$. Note that in this optimization problem, the constraint of Eq. (15c) is only active for LMPC 3 and LMPC 2; and the constraint of Eq. (15d) is only active for LMPC 2 and LMPC 1. The constraint of Eq. (15g) is used to make sure that each controller has a minimum contribution to the decrease rate of the Lyapunov function which is used to guarantee the closed-loop stability. Once all optimization problems are solved, the manipulated inputs of the distributed LMPC system are defined as follows:

$$u_i^L(t|x) = u_i^*(t - t_k | t_k), \quad i = 1,2,3,\ \forall t \in [t_k, t_{k+1}).$$

The alkylation process under this DMPC scheme with inputs defined by $u_i = u_i^L$, $i=1,2,3$, maintains the same stability region as the Lyapunov-based control law h (Liu et al., 2009, 2010).

3.2. Fault detection and isolation

We consider control actuator faults that can be detected and isolated by an appropriate nonlinear dynamic filter by observing the evolution of the closed-loop system state. This consideration requires that a fault in a control actuator influences the evolution of at least one of the states. In order to isolate the occurrence of a fault, it is further required that the control actuator in question is the only one influencing a certain set of the system states (i.e., each fault has a unique fault signature), see Table 5. For more discussions on systems having isolable structures, see (Mhaskar et al., 2008; Ohran et al., 2008).

Table 5
Fault signature shows which residuals are triggered by faults in particular actuators. Note that some signatures overlap (i.e., Q_2 fault signature overlaps with F_4 fault signature and Q_3 fault signature overlaps with F_6 fault signature).

Actuator	Fault signature
Q_1	T_1
Q_2	T_2
Q_3	T_3
Q_4	T_4
Q_5	T_5
F_4	$T_2, C_{A2}, C_{B2}, C_{C2}$
F_6	$T_3, C_{A3}, C_{B3}, C_{C3}$

The DMPC system of Eq. (15) is the control configuration for the fault-free system of Eq. (14). We first design an FDI scheme to detect faults in this control system. In this FDI scheme, a filter is designed for each state and the design of the filter for the pth, $p=1,\ldots,25$, state in the system state vector x is as follows:

$$\dot{\hat{x}}_p(t) = f_p(X_p) + \sum_{i=1}^{3} g_{ip}(X_p) u_i^L(X_p) \tag{16}$$

where $\hat{x}_p$ is the filter output for the pth state, f_p and g_{ip} are the pth components of the vector functions f and g_i, respectively. With a slight abuse of notation, we have dropped the time index in Eq. (16) in the control functions and denote $u_i^L(t|x)$ with $u_i^L(x)$, in order to simplify the FDI definitions. The state X_p is obtained from both the actual state measurements, x, and the filter output, $\hat{x}_p$, as follows:

$$X_p(t) = [x_1(t),\ldots,x_{p-1}(t), \hat{x}_p(t), x_{p+1}(t),\ldots,x_{25}(t)]^T$$

Note that in the filter of Eq. (16), the control inputs $u_i^L(X_p)$ are determined by the same LMPC of Eq. (15) as applied to the actual process, and are updated at every sampling time (i.e., the sampling time instants $\{t_{k\ge 0}\}$).

The states of the FDI filters are initialized at $t=0$ to the actual state values; that is, $\hat{x}_p = x_p$. The FDI filters are only initialized at $t=0$ such that $\hat{x}_p(0) = x_p(0)$. The information generated by the filters provides a fault-free estimate of the process at any time t and allows detection of the faults. For each state associated with a filter, the FDI residual can be defined as:

$$r_p(t) = |\hat{x}_p(t) - x_p(t)|$$

with $p=1,\ldots,25$. The residual r_p is computed continuously because $\hat{x}_p(t)$ is known for all t and the state measurement, x, is also available for all t. If no fault occurs, the filter states track the system states. In this case, the dynamics of the system states and the FDI filter states are identical, so $r_p(t)=0$ for all times. When there is a fault in the system, filter residuals affected directly by the fault will deviate from zero soon after the occurrence of the fault. For more detailed discussion on the properties of the filters, see Mhaskar et al. (2008).

Note that due to sensor measurement and process noise, the residuals will be nonzero even without an actuator fault. This necessitates the use of fault detection thresholds so that a fault is declared only when a residual exceeds a specific threshold value, σ_p. This threshold value is chosen to avoid false alarms due to process and sensor measurement noise, but should still be sensitive enough to detect faults in a timely manner so that effective fault-tolerant control can be performed.

The objective of the FDI scheme is to quickly detect an actuator fault when it occurs, and then identify which of the possible different actuator faults has occurred. When a fault occurs, one or more of the filter residuals will become nonzero. Once a residual (r_p) is detected at time t_{σ_p}, the monitoring system will declare a fault alarm. In order to isolate a fault, the system must have an isolable structure in which different faults have different fault signatures. In some cases the fault signatures overlap such that a waiting time (Δt_i) is used to confidently distinguish between fault signatures by letting the fault propagate in the system (see Table 5 where a Q_2 fault signature overlaps with an F_4 signature). The time Δt_i is chosen to achieve a trade off between quicker reconfiguration and the need to confidently isolate a fault and is based on the worst case time needed for the slowest actuator fault to develop its fault signature. If a fault is isolated, the FDIFTC system will send the fault information and reconfiguration policy to the distributed controllers to activate the FTC system as shown in Fig. 3.

3.3. Fault parameter estimation

After a fault has been isolated, the FTC system must know the magnitude of the fault in order to target the corresponding new operating point and properly stabilize the system in the presence of the fault. To simplify the description of the proposed method, we consider faults of constant magnitudes in this work; however, faults with slowly time-varying values can be handled using the proposed FDIFTC method in a straightforward manner.

When a residual (r_p) exceeds its threshold (σ_p), we begin to collect the sampled system states as well as the actual control inputs applied to the system. When the fault is confirmed and isolated, a least square optimization problem is solved to estimate the magnitude of the fault based on the sampled system states and the actual control inputs. Specifically, we collect the sampled system states, $x(t)$, and record the actual control inputs (i.e., $u_1(t)=u_1^L(t),\ldots,u_3(t)=u_3^L(t)$) applied to the system from t_{σ_p} to the fault isolation time ($t_{isolate}=t_{\sigma_p}+\Delta t_i$). The magnitude of the fault (denoted as d) is estimated by solving the following optimization problem:

$$\min_{d} \quad \sum_{i=0}^{M}(x(t_f+i\Delta)-\tilde{x}(t_f+i\Delta))^2 \tag{17a}$$

$$\text{s.t.} \quad \dot{\tilde{x}}(t)=f(\tilde{x}(t))+g(\tilde{x}(t))(u^L(t)+\tilde{u}) \tag{17b}$$

$$\tilde{x}(t_f)=x(t_f) \tag{17c}$$

where $\tilde{u}=[0\ \cdots\ d\ \cdots\ 0]^T$ is the fault vector, $u^L(t)=[u_1^L(t)^T\ \ldots\ u_3^L(t)^T]^T$ is the actual control inputs that have been applied to the closed-loop system from t_{σ_p} to $t_{isolate}$, M is the maximum integer satisfying $M\Delta \le t_{isolate}-t_{\sigma_p}$, and $x(t_{\sigma_p})$ is the system state at the fault detection time. The solution to the optimization problem of Eq. (17) is denoted by d^*, which is the estimate of the actual fault from a least-square point of view.

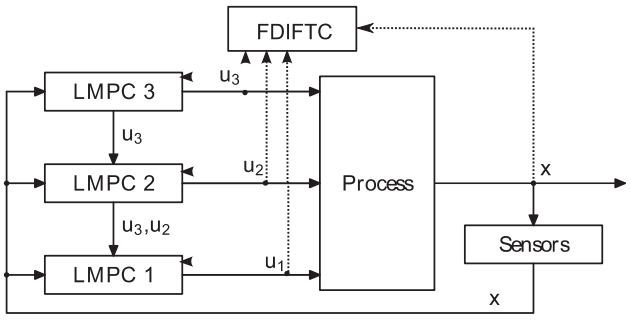

Fig. 3. Sequential distributed LMPC with FDIFTC system.

3.4. FTC consideration and strategies

In order to carry out FTC, there must be a backup control configuration for the system under consideration. For the alkylation process, the presence of the control action u_3 brings extra control flexibility to the closed-loop system which can be used to carry out FTC. From extensive simulations, we found that the closed-loop process can also be stabilized using the manipulated input sets $\{u_{11},u_{12},u_2,u_3\}$ and $\{u_1,u_2,u_{31}\}$ when the faults in u_{13} and u_{32} are small enough such that the new operating points are close enough to the original operating point. This fact can be taken as an advantage to design FTC systems for the alkylation process.

First, we discuss the case that there is a persistent fault d_1 in u_{13}. In this case, we need to design a Lyapunov-based control law $h_2(x)$ which manipulates u_{11}, u_{12}, u_2 and u_3 to stabilize the closed-loop process. The control law $h_2(x)$ in Sontag (1989) and its expression is omitted for brevity. This control law will be used in the backup distributed LMPC when the fault in u_{13} is detected and isolated. We still design three LMPC controllers in the backup DMPC system. One LMPC is used to manipulate u_{11} and u_{12}, one for u_2, and the third is used to manipulate u_3. In this backup DMPC system, the three LMPCs coordinate their actions to maintain the closed-loop stability. We refer to the LMPC manipulating u_{11} and u_{12} as the backup LMPC 1 and the LMPC manipulating u_2 and u_3 as the backup LMPC 2 and 3, respectively. The three backup LMPCs are also evaluated in sequence. Specifically, the backup LMPC 3 is designed as follows:

$$\min_{u_3\in S(\Delta)} \int_0^{N\Delta}\left[\tilde{x}(\tau)^T Q_c\tilde{x}(\tau)+\sum_{i=1}^{3}u_i(\tau)^T R_{ci}u_i(\tau)\right]d\tau$$

$$\dot{\tilde{x}}(\tau)=f(\tilde{x}(\tau))+\sum_{i=1}^{3}g_i(\tilde{x}(\tau))u_i(\tau) \tag{18a}$$

$$u_2(\tau)=h_{22}(\tilde{x}(j\Delta)), \tag{18b}$$

$$[u_{11}(\tau)\ u_{12}(\tau)]^T=h_{21}(\tilde{x}(j\Delta)),\quad \forall\tau\in[j\Delta,(j+1)\Delta),\ j=0,\ldots,N-1 \tag{18c}$$

$$u_{13}(\tau)=0 \tag{18d}$$

$$\tilde{x}(0)=x(t_k) \tag{18e}$$

$$u_3(\tau)\in U_3 \tag{18f}$$

$$\frac{\partial V(x)}{\partial x}g_3(x(t_k))u_3(0)\le\frac{\partial V(x)}{\partial x}g_3(x(t_k))h_{23}(x(t_k)). \tag{18g}$$

The solution to the optimization problem of Eq. (18) is denoted as $u_3^{b*}(t|t_k)$. The backup LMPC 2 optimizes u_2 and is designed as follows:

$$\min_{u_2\in S(\Delta)} \int_0^{N\Delta}\left[\tilde{x}(\tau)^T Q_c\tilde{x}(\tau)+\sum_{i=1}^{3}u_i(\tau)^T R_{ci}u_i(\tau)\right]d\tau \tag{19a}$$

$$\dot{\tilde{x}}(\tau)=f(\tilde{x}(\tau))+\sum_{i=1}^{2}g_i(\tilde{x}(\tau))u_i(\tau)+g_3(\tilde{x}(\tau))u_3^{b*}(\tau) \tag{19b}$$

$$[u_{11}(\tau)\ u_{12}(\tau)]^T=h_{21}(\tilde{x}(j\Delta)),\quad \forall\tau\in[j\Delta,(j+1)\Delta), \tag{19c}$$

$$j=0,\ldots,N-1 \tag{19d}$$

$$u_{13}(\tau)=0 \tag{19e}$$

$$\tilde{x}(0)=x(t_k) \tag{19f}$$

$$u_2(\tau)\in U_2 \tag{19g}$$

$$\frac{\partial V(x)}{\partial x}g_2(x(t_k))u_2(0)\le\frac{\partial V(x)}{\partial x}g_2(x(t_k))h_{22}(x(t_k)). \tag{19h}$$

The solution to the optimization problem of Eq. (19) is denoted as $u_2^{b*}(t|t_k)$. The backup LMPC 1 optimizes u_{11} and is designed as follows:

$$\min_{u_1 \in S(\Delta)} \int_0^{N\Delta} \left[\tilde{x}(\tau)^T Q_c \tilde{x}(\tau) + \sum_{i=1}^{3} u_i(\tau)^T R_{ci} u_i(\tau) \right] d\tau \tag{20a}$$

$$\dot{\tilde{x}}(t) = f(\tilde{x}(t)) + g_1(\tilde{x}(t))[u_{11}(t)\ u_{12}(t)\ 0]^T + \sum_{i=2}^{3} g_i(\tilde{x}(t)) u_i^{b*}(t) \tag{20b}$$

$$\tilde{x}(t_k) = x(t_k) \tag{20c}$$

$$u_1(t) \in U_1 \tag{20d}$$

$$u_{13}(t) = 0 \tag{20e}$$

$$\frac{\partial V_2(x)}{\partial x} g_1(x(t_k))[u_{11}(t)\ u_{12}(t)\ 0]^T \le \frac{\partial V_2(x)}{\partial x} g_1(x(t_k))[h_{21}(x(t_k))^T\ 0]^T. \tag{20f}$$

The solution to the optimization problem of Eq. (20) is denoted as $u_{11}^{b*}(t|t_k)$. The control inputs of the backup DMPC system are defined as follows:

$$[u_{11}^b(t)\ u_{12}^b(t)]^T = [u_{11}^{b*}(t|t_k)\ u_{12}^{b*}(t|t_k)], \quad \forall t \in [t_k, t_{k+1})$$

$$u_{13}^b(t) = 0, \quad \forall t$$

$$u_2^b(t) = u_2^{b*}(t|t_k), \quad \forall t \in [t_k, t_{k+1})$$

$$u_3^b(t) = u_3^{b*}(t|t_k), \quad \forall t \in [t_k, t_{k+1})$$

The fault-free closed-loop system of Eq. (14) under the backup DMPC control with inputs defined by $u_{11} = u_{11}^b$, $u_{12} = 0$, $u_2 = u_2^b$, and $u_3 = u_3^b$ maintains practical stability of the closed-loop system because of the Lyapunov-based constraints of Eqs. (18g) (19h) and (20f) (Liu et al., 2010).

When a fault in u_{13} is detected, isolated and the magnitude of the fault is estimated, suitable FTC strategies can be carried out to keep the closed-loop system state within a desired operating region. Because of the fault, the operating point of the fault-free system may not be achievable because of the input constraints and the system structure. In this case, we may operate the system at a new operating point within the desired operating region. To determine the new operating point x_s, we propose to solve an optimization problem. Specifically, when the fault is d_1^*, the new operating point, x_s, is obtained by solving the following optimization problem:

$$\min_{x_s, u_s} x_s^T W x_s \tag{21a}$$

$$\text{s.t. } f(x_s) + g(x_s)(u_s + \tilde{u}) = 0 \tag{21b}$$

$$u_s + \tilde{u} \in U \tag{21c}$$

$$x_s \in X \tag{21d}$$

where W is a positive weighting matrix, $\tilde{u} = [0\ \cdots\ d_1^*\ \cdots\ 0]^T$ and X denotes the desired operating state-space region. The objective of the above optimization problem is to find an operating point within the desired operating state-space region such that the distance (measured by weighted Euclidean norm) between the new operating point and the original (fault-free) operating point is minimized. We assume that the optimization problem of Eq. (21) is always feasible which implies that we can always find the new operating point x_s and the corresponding new steady-state control input values $u_s = [u_{1s}^T\ u_{2s}^T\ u_{3s}^T]^T$.

Once the fault is isolated, the FTC strategy would shut down the control action of u_{13} and reconfigure the DMPC algorithms of Eq. (15) to the backup DMPC of Eqs. (18)–(20) to manipulate u_{11}, u_{12}, u_2, and u_3 to control the process. In order to maintain the stability of the closed-loop system, the designs of the three backup LMPCs and the design of $h_2(x)$ needs to be updated with the new operating point and the corresponding new steady-state control input values; as well as being updated with the fault magnitude information. Note that the proposed method is only one of many possible approaches to determine the new operating point in the case of a fault. The basic idea of the proposed method is to find a new operating point that stays as close as possible to the original operating point.

Next, we consider the case that there is a persistent fault d_3 in u_{32}. In this case, if the fault is detected and isolated in a reasonable time frame, it is possible to switch off the faulty portion of LMPC 3 and only use u_1, u_2, and u_{31} in the control system of Eq. (15). When u_{32} is switched off from the closed-loop system, u_{32} is set to the fault value (i.e., $u_{32} = d_3$). In order to maintain the stability of the closed-loop system, the design of LMPC 1, 2, 3, and $h(x)$ will be updated with the new operating point, corresponding to the new steady-state control input values, and updated with the fault magnitude information (i.e., $u_{32} = d_2$). The control inputs determined by the updated LMPC 1, 2, and 3 will be referred to as $u_1'(x)$, $u_2'(x)$, and $u_3'(x)$. This FTC strategy will maintain the closed-loop stability if implemented quickly enough such that the state of the closed-loop system is still within the stability region of the backup controllers and parameter estimation is sufficiently accurate, however, the performance of the closed-loop system may degrade to some extent.

However, when there is a fault in u_{11}, or u_{12} or u_2 or u_{31}, it may be impossible to successfully carry out FTC without activating backup actuators within the DMPC systems for the alkylation process considered in this work.

The FTC switching rules for the alkylation process within the DMPC system of Eq. (15) are described as follows:

1. When a fault in the actuator associated with u_{32} is isolated at t_f, the FTC switching rule is:

$$u_1(t) = \begin{cases} u_1^L(x), & t \le t_f \\ u_1''(x), & t > t_f \end{cases} \tag{22a}$$

$$u_2(t) = \begin{cases} u_2^L(x), & t \le t_f \\ u_2''(x), & t > t_f \end{cases} \tag{22b}$$

$$u_3(t) = \begin{cases} u_3^L(x), & t \le t_f \\ \begin{bmatrix} u_{31}''(x) \\ d_3 \end{bmatrix}, & t > t_f \end{cases} \tag{22c}$$

2. When a fault in the actuator associated with u_{13} is detected at t_f, the FTC switching rule is:

$$u_1(t) = \begin{cases} u_1^L(x), & t \le t_f \\ \begin{bmatrix} u_{11}^b(x) \\ u_{12}^b(x) \\ d_1 \end{bmatrix}, & t > t_f \end{cases} \tag{23a}$$

$$u_2(t) = \begin{cases} u_2^L(x), & t \le t_f \\ u_2^b(x), & t > t_f \end{cases} \tag{23b}$$

$$u_3(t) = \begin{cases} u_3^L(x), & t \le t_f \\ u_3^b(x), & t > t_f \end{cases} \tag{23c}$$

Remark 1. Note that in the simulations in Section 4, we do not explicitly compute the stability regions for the new operating points. The time delay introduced by the calculation of the stability regions in the FTC system (note that this calculation

should be done on-line) may deteriorate the performance of the FTC system especially for large-scale nonlinear systems. Instead, we pick the thresholds of the residuals based on extensive normal (fault-free) process operation data and off-line simulations to make the FTC system to respond quickly enough to a fault (so that the process state is still within the corresponding stability region) and to minimize the occurrence of false alarms due to measurement noise and process noise. An alternative to the above approach is to compute off-line some temporary operating points with well characterized stability regions and then optimally choose an appropriate temporary operating point when a fault occurs, following the approach in Du et al. (2012), Gandhi and Mhaskar (2008).

Remark 2. Note that in the design of the FDI/FTC reconfiguration strategy, uncertainties (e.g., sensor noise, process noise) are explicitly taken into account. The design of the FDI filters can tolerate certain level of sensor noise and process noise if the threshold values are chosen appropriately. A least square approach is adopted to estimate the new operating point once a fault is detected and isolated, which also takes into account the effect of actuator fault—another form of process uncertainty. The utilized controllers have also been proved to be robust to bounded noise and disturbances. Moreover, if the process structure and the corresponding faults satisfy certain isolability conditions, the actuator faults are guaranteed to be detected and isolated using the filter design adopted in this work. Refer to Mhaskar et al. (2008) for a verifiable condition on the process structure and the corresponding faults. We also note that the FDI scheme adopted in this work is just one of the many possible approaches. Any FDI schemes that account for nonlinear systems and provide quick fault detection and isolation (e.g, Zhang et al., 2012, 2010) could be possibly adopted in the present FDI/FTC strategy.

4. Simulation results

In this section, various simulations are presented with the goal of showing the abilities of the fault detection/isolation and fault tolerant control system along with its limitations. First, we demonstrate the closed-loop system poor performance upon the triggering of an actuator fault with no fault tolerant control implemented. In the second simulation we again trigger the same fault and demonstrate the timely fault detection and isolation of the fault and triggering of the fault tolerant control system to reconfigure the control system to maintain stability of the plant with a persistent actuator fault present. Varying levels of recovery are possible after isolation of an actuator fault depending on the robustness of the remaining control structure, and the speed and flexibility of the FDI/FTC system. Note that in this section, we consider faults that make the actuator stuck at certain values (i.e., $u+\tilde{u}=c$ with c a constant). The aforementioned approach can be applied to this case in a straightforward manner.

4.1. No fault tolerant control implementation

The first two plots presented show the trajectory of the plant under no-fault conditions. In Figs. 4 and 5 we see the plant's temperatures (T) and ethylene concentrations (C_B) begin near the steady state (dotted line) and are considered stabilized around the steady state by the 200 min mark. We found that besides vessel temperature, focusing only on the ethylene concentration provided the necessary confidence in demonstrating and isolating actuator faults for this particular plant. Since in this particular process (see Table 5) the Q_2 actuator and the F_4 actuator partially overlap in terms of their fault signatures since they both trigger

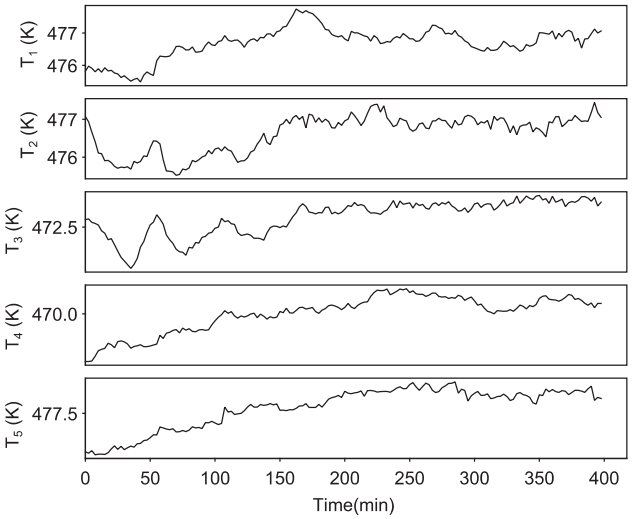

Fig. 4. Temperature trajectories for the five vessels under normal fault free operation. Dotted line represents target operating point. The process reaches steady-state conditions around 200 min.

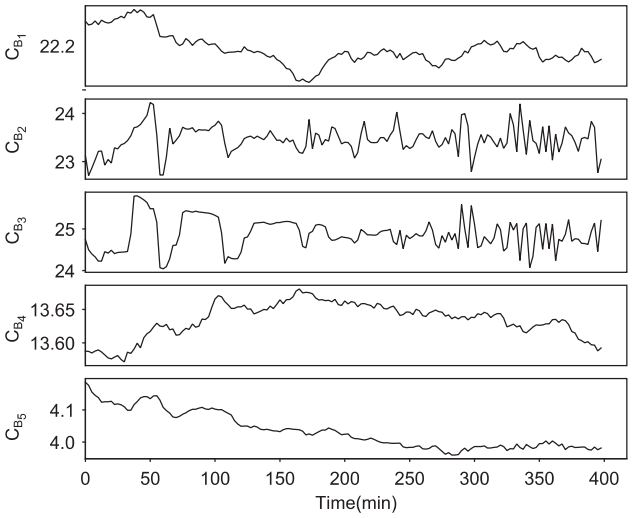

Fig. 5. Trajectories of ethylene concentration (mol/m^3) for the five vessels under normal fault free operation. Dotted line represents target operating point. The process reaches steady state after 200 min.

the vessel 2 temperature residual (r_{T_2}) and the difference being that the F_4 also triggers the concentration residuals. Similarly a Q_3 fault overlaps with a F_6 fault. In simulations ethylene (C_b) was consistently the first of the concentration residuals to respond from a flow actuator fault (F_2 and F_4). As such it is sufficient to monitor the temperatures and each vessel's ethylene concentration in order to properly isolate an actuator fault. In simulations where a fault is considered, the unknown actuator fault is triggered at the 200 min mark and the fault is set to +50% of its maximum actuation, unless written otherwise. Noise was introduced to the closed-loop system as process noise and measurement noise.

The first simulation considered has a fault triggered in the heat actuator of vessel 3 (Q_3) that shows the closed-loop system moving quickly away from the target steady states in Fig. 6. The Q_3 actuator fault is triggered at 200 min and increased the heat delivered to vessel 3 where the first residual to consistently exceed its threshold for Δt_i is vessel 3 temperature (r_{T_3}) at

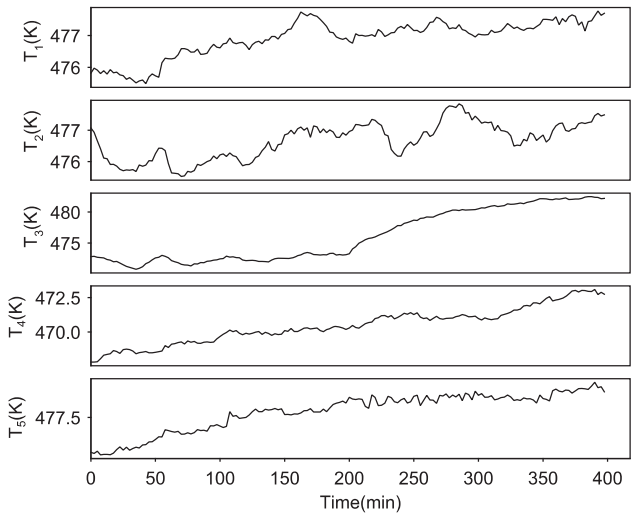

Fig. 6. Temperature trajectories of the five vessels after triggering a Q_3 fault at time 200 min with no fault tolerant control. Note that the vessel 3 disturbance eventually propagates downstream to vessels 4 and 5 after 310 min and 360 min, respectively.

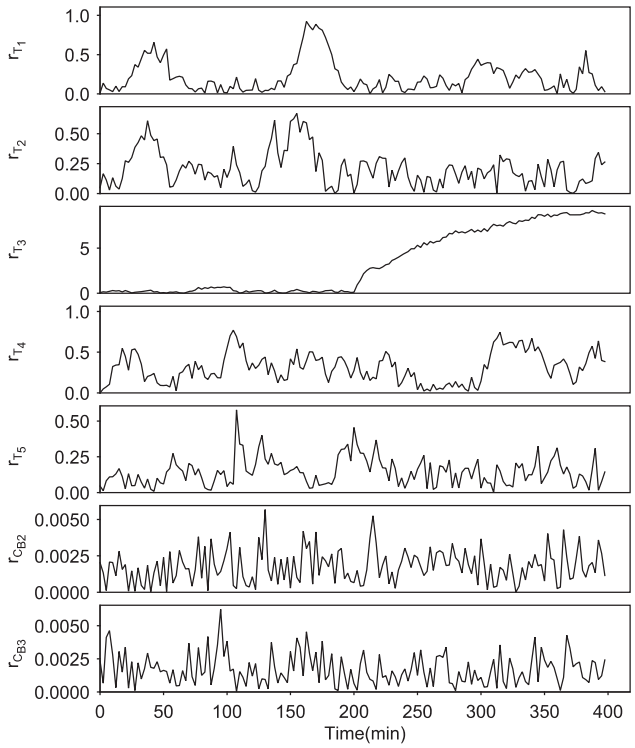

Fig. 7. Residual plots of key isolation residuals showing residual pattern upon triggering a fault in the heat actuator to the third vessel (Q_3) with no fault tolerant control. Note how only the residual associated with the temperature of vessel 3 (r_{T_3}) is severely affected.

202 min shown in Fig. 7. The residual response is consistent with the plant model filter design where only the filter states directly associated with the fault will show an immediate deviation as shown in Eq. (1). Fig. 6 shows the temperature in vessel 3 (T_3) increasing beyond its target shortly after initiation of the heat actuator fault and the fault manifesting in vessel 4 temperature after the 310 min mark when no fault tolerant control is implemented. The final cost of the simulation without fault tolerant control is 9.9×10^7 units.

4.2. FTC of a Q_3 heat actuator fault

In the next example we look at how the fault tolerant control system responds to the same heat actuator (Q_3) fault at 200 min. The fault's first appearance is most evident in the residual plot in Fig. 8 where vessel 3 temperature residual spikes upward after 202 min (t_{σ_p}). At this time the fault isolation system performs two actions, first it begins monitoring the residuals for a consistent fault signature where the appropriate residuals exceed their thresholds for a specified amount of time (Δt_i) and the fault is isolated. The second action after detecting a possible fault is to begin logging plant states and controller action in order for successful fault estimation to be achieved as presented in Section 3.3. The isolation time ($\Delta t_i =$ 10 plant steps $= 150$ sec) was determined from various simulations by initiating a low magnitude fault and recording the necessary time for a consistent fault signature. The value was chosen long enough to confidently isolate to a certain degree of certainty and short enough so that the fault tolerant control system can stabilize the plant by reconfiguring the control system while the plant remains in the stability region of the reconfigured control system. A low magnitude fault was used as these typically have the slowest propagation within the system and represents a worst case in terms of isolation time. In the event of losing a fault signature (i.e., the corresponding residual recedes below the threshold) within the isolation time Δt_i, the fault isolation process is reset.

At the end of the isolation time ($t_{\sigma_p} + \Delta t_i = 202$ min $+$ 150 sec $=$ 205 min) the Q_3 fault is isolated and the magnitude is correctly estimated at 50% of maximum actuation. This information is used to reconfigure the control system to account for the persistent disturbance. The successful reconfiguration is obvious at the 205 min mark in Figs. 8 and 9 where the vessel 3 temperature residual (r_{T_3}) dives down below the threshold and the temperature (T_3) returns to its steady state. But note that after isolation the residuals do not provide useful information unless further reconfiguration strategies are built into the fault tolerant control system. The size of the small spike in T_3 is directly related to the isolation time but it is required in order to confidently isolate when fault signatures have overlapping residual patterns. Reconfiguration in this case is due to the flexibility in the control system to ramp up the F_6 flow actuator to compensate for the problem with Q_3. The final cost of the simulation with fault tolerant control is 2.2×10^7 units.

4.3. FTC of an F_4 flow actuator fault

In the very last example we look at a fault in the flow actuator to vessel two (F_4) at 100% maximum actuation which introduces pure ethylene (C_b) into vessel 2, with no fault tolerant control. Because of the structure of the plant we expect the fault to affect more than one residual, in fact all residuals associated with vessel 2. In Fig. 10, we see that the pattern of the residual for concentration of ethylene in vessel 2 changes shortly after the fault is triggered in F_4. In this example with no fault tolerant control, the fault propagates and we see that the temperatures for tanks 2 and 3 begin to change after 200 min in Fig. 11.

In the last set of figures we implement the appropriate FTC strategy after isolation of a flow actuator fault in vessel 2 (F_4). After the fault is triggered at 200 min the temperature in vessel 2 moves away from the target steady state (Fig. 14). The first residual to trigger monitoring is the ethylene concentration in tank 2 ($r_{C_{B2}}$) at 200 min (Fig. 15). The fault is isolated and FTC reconfiguration is initiated at time 203 min where we see that the vessel 2 temperature plot begin to shift back towards the original steady state as it did in Fig. 11. Comparing the temperatures and

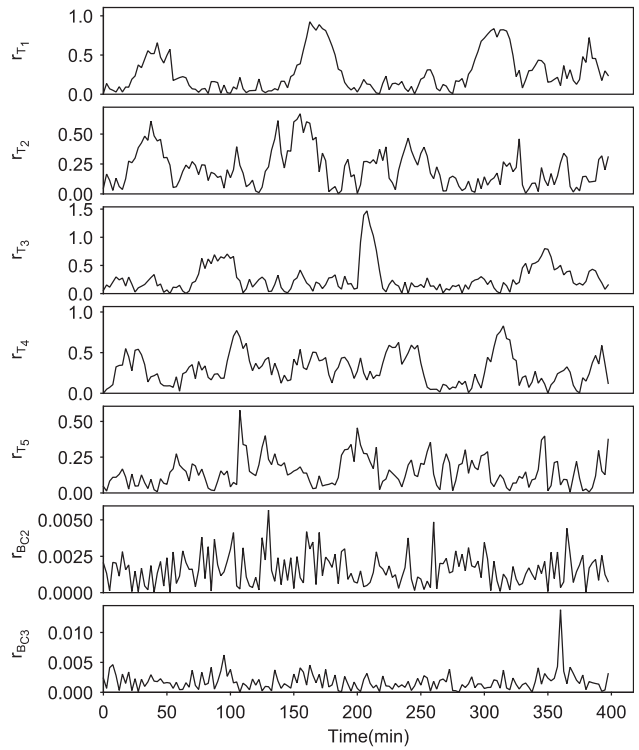

Fig. 8. Residual plots of key isolation residuals showing residual pattern upon triggering a fault in the heat actuator to the third vessel (Q_3) and using FTC at time 205 min. Note how residual r_{T_3} trajectory changes immediately after reconfiguration.

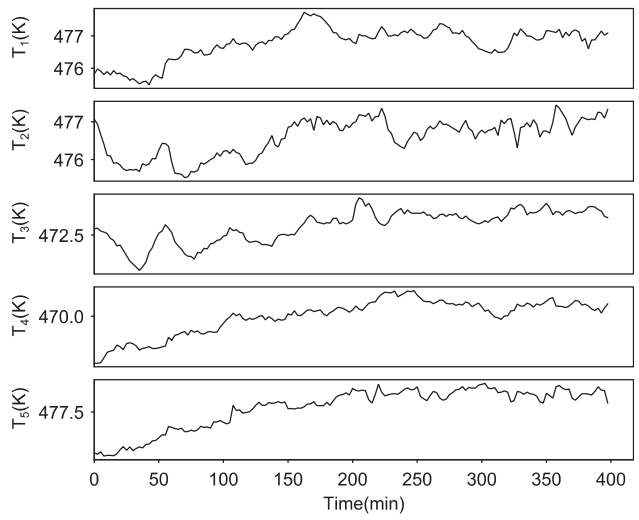

Fig. 9. Temperature trajectories of the five vessels after triggering a Q_3 actuator fault at 200 min and achieving fault isolation at 205 min. The small peak above the threshold in T_3 from 200 to 210 min is the result of the actuator fault.

ethylene concentration plots under fault tolerant control and no fault tolerant control, the difference is minor. But comparing the cost for the no fault tolerant control simulation (Fig. 12) with a cost of 6.3×10^7 units and the fault tolerant control simulation (Fig. 13) with a final cost of 5.3×10^7 units shows a significant gain and is partly due to a reduction in wasted control action (compare Figs. 12 and 13).

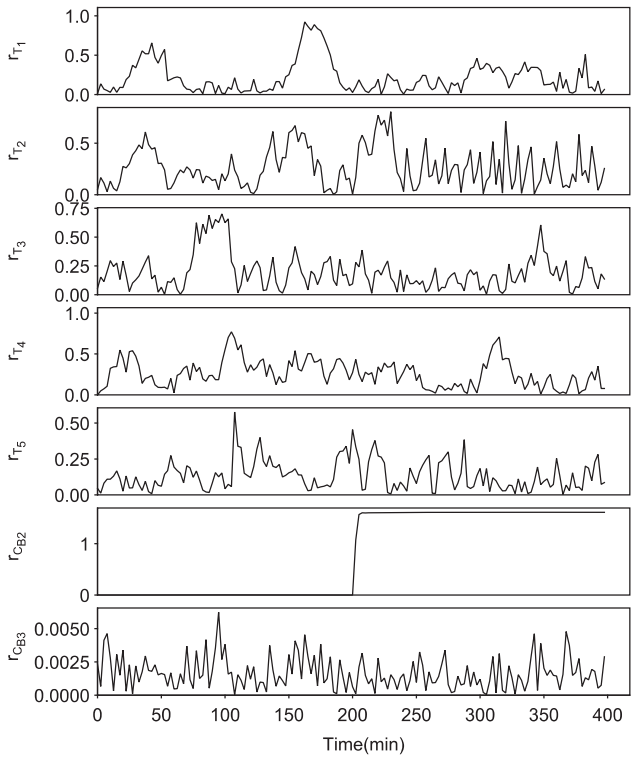

Fig. 10. Residual plots after initiating a flow actuator fault in tank 2 (F_4) with no fault tolerant control. Note that this fault causes a shift in the residuals for tank 2 ethylene concentration at 200 min.

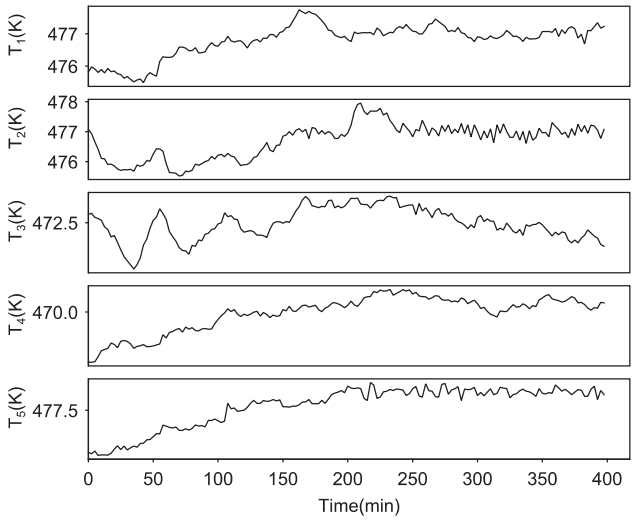

Fig. 11. Temperature trajectories of the five vessels after triggering a F_4 fault at time 200 min with no fault tolerant control.

In the case where an actuator fault occurs in vessel one, four, or five, the fault will be properly isolated and estimated, but due to the plant structure, there does not exist a way to compensate for the lost actuation and persistent disturbance. Also due to the persistent fault and the structure of the process, the original target operating point is not accessible anymore, and the new target steady state is chosen as to remain as close to the original target with the persistent fault present.

The simulations were carried out using Java programming language on a Pentium 3.20 GHz computer. The optimization

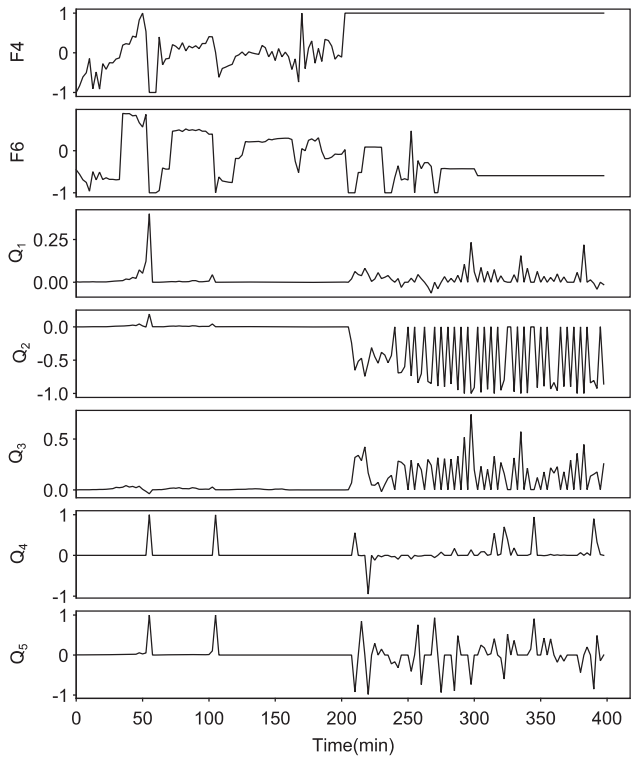

Fig. 12. Manipulated input trajectories after initiating a flow actuator fault in tank 2 (F_4) with no fault tolerant control. Final cost 6.7×10^7 units. Units of F_4 are m^3/s and $Q_1,\ldots,Q_5$ are J/s; all inputs are scaled to be in the range of $[-1,1]$ using the values of Table 4.

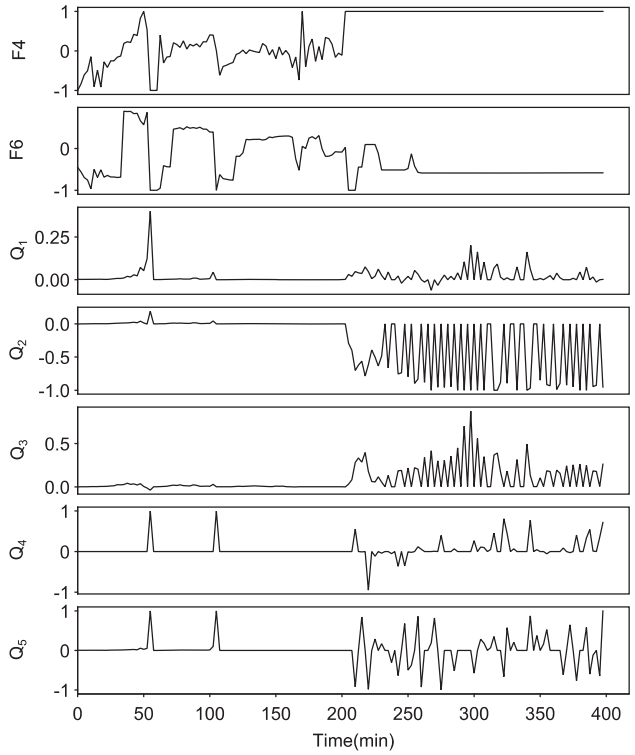

Fig. 13. Manipulated input trajectories after initiating a flow actuator fault in tank 2 (F_4) with fault tolerant control. Final cost 5.3×10^7 units. Units of F_4 are m^3/s and $Q_1,\ldots,Q_5$ are J/s; all inputs are scaled to be in the range of $[-1,1]$ using the values of Table 4.

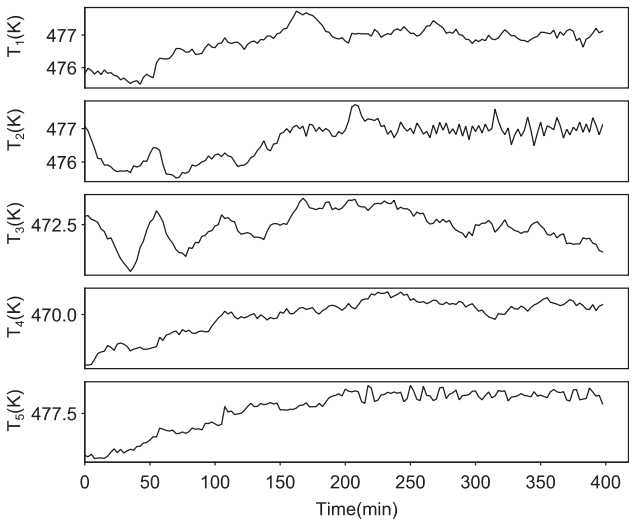

Fig. 14. Temperature trajectories of the five vessels after triggering a F_4 fault at time 200 min with FTC reconfiguration. Note smaller deviation peak in T_2 compared to no FTC implementation in Fig. 11.

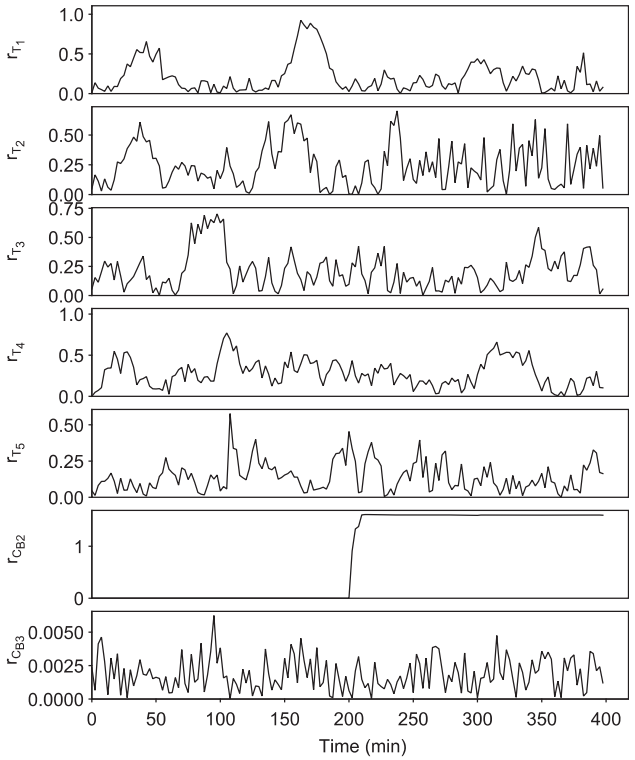

Fig. 15. Residual plots after initiating a flow actuator fault in tank 2 (F_4) with fault tolerant control.

problems were solved using the open source interior point optimizer Ipopt (Wächter and Biegler, 2006).

5. Conclusion

In this work, we focused on fault detection, isolation and fault tolerant control of an alkylation of benzene process under distributed model predictive control in the presence of an

unknown actuator fault. In order to achieve the objectives of closed-loop stability and optimal plant operation, methods for quick fault detection and isolation were necessary such that the faults perturbation had not yet pushed the plant state outside the reconfigured control system's stability region. In addition accurate fault estimation and optimal recalculation of state and input targets was necessary to maintain optimal plant operation in terms of cost. We demonstrated that FTC reconfiguration benefits were most visible in the total operating cost, where controller action no longer wasted energy by under- and over- compensating for an unresponsive and disruptive actuator.

References

Camponogara, E., Jia, D., Krogh, B.H., Talukdar, S., 2002. Distributed model predictive control. IEEE Control Syst. Mag. 22, 44–52.

Chilin, D., Liu, J., Muñoz de la Peña, D., Christofides, P.D., Davis, J.F., 2010. Detection, isolation and handling of actuator faults in distributed model predictive control systems. J. Process Control 20, 1059–1075.

Chilin, D., Liu, J., Davis, J.F., Christofides, P.D., 2012. Data-based monitoring and reconfiguration of a distributed model predictive control system. Int. J. Robust Nonlinear Control 22, 68–88.

Christofides, P.D., Scattolini, R., Muñoz de la Peña, D., Liu, J., 2012. Distributed model predictive control: a tutorial review. Proc. Chem. Process Control 8, 22pp. (Savannah, Georgia).

Du, M., Nease, J., Mhaskar, P., 2012. An integrated fault diagnosis and safe-parking framework for fault-tolerant control of nonlinear systems. Int. J. Robust Nonlinear Control 22, 105–122.

Gandhi, R., Mhaskar, P., 2008. Safe-parking of nonlinear process systems. Comput. Chem. Eng. 32, 2113–2122.

Ganji, H., Ahari, J.S., Farshi, A., Kakavand, M., 2004. Modelling and simulation of benzene alkylation process reactors for production of ethylbenzene. Pet. Coal 46, 55–63.

Lee, W.J., 2005. Ethylbenzene Dehydrogenation Into Styrene: Kinetic Modeling and Reactor Simulation. Ph.D. Thesis. Texas A&M University, College Station, TX, USA.

Liu, J., Muñoz de la Peña, D., Christofides, P.D., 2009. Distributed model predictive control of nonlinear process systems. AIChE J. 55, 1171–1184.

Liu, J., Chen, X., Muñoz de la Peña, D., Christofides, P.D., 2010. Sequential and iterative architectures for distributed model predictive control of nonlinear process systems. AIChE J. 56, 2137–2149.

Mhaskar, P., Gani, A., El-Farra, N.H., McFall, C., Christofides, P.D., Davis, J.F., 2006. Integrated fault-detection and fault-tolerant control of process systems. AIChE J. 52, 2129–2148.

Mhaskar, P., McFall, C., Gani, A., Christofides, P.D., Davis, J.F., 2008. Isolation and handling of actuator faults in nonlinear systems. Automatica 44, 53–62.

Ohran, B., Muñoz de la Peña, D., Christofides, P.D., Davis, J.F., 2008. Enhancing data-based fault isolation through nonlinear control. AIChE J. 54, 223–241.

Perego, C., Ingallina, P., 2004. Combining alkylation and transalkylation for alkylaromatic production. Green Chem. 6, 274–279.

Perk, S., Teymour, F., Cinar, A., 2010. Statistical monitoring of complex chemical processes using agent-based systems. Ind. Eng. Chem. Res. 17, 5080–5093.

Rawlings, J.B., Stewart, B.T., 2008. Coordinating multiple optimization-based controllers: new opportunities and challenges. J. Process Control 18, 839–845.

Scattolini, R., 2009. Architectures for distributed and hierarchical model predictive control - a review. J. Process Control 19, 723–731.

Sontag, E., 1989. A 'universal' construction of Artstein's theorem on nonlinear stabilization. Syst. Control Lett. 13, 117–123.

Tatara, E., Cinar, A., Teymour, F., 2007. Control of complex distributed systems with distributed intelligent agents. J. Process Control 17, 415–427.

Wächter, A., Biegler, L.T., 2006. On the implementation of primal-dual interior point filter line search algorithm for large-scale nonlinear programming. Math. Programming 106, 25–57.

Woodle, G.B., 2006. Petrochemicals and petrochemical processing. Ethylbenzene, vol. I. Taylor & Francis Group, New York, pp. 929–941.

You, H., Long, W., Pan, Y., 2006. The mechanism and kinetics for the alkylation of benzene with ethylene. Pet. Sci. Technol. 24, 1079–1088.

Zhang, Y., Zhou, H., Qin, S.J., Chai, T., 2010. Decentralized fault diagonosis of large-scale processes using multiblock kernel partial least squares. IEEE Trans. Ind. Inf. 6, 3–10.

Zhang, Y., Chai, T., Li, Z., 2012. Modeling and monitoring of dynamic processes. IEEE Trans. Neural Netw. Learn. Syst. 23, 277–284.